Journal of Biomechanics 43 (2010) 1689–1695

Contents lists available at ScienceDirect

Journal of Biomechanics

journal homepage: www.elsevier.com/locate/jbiomech
www.JBiomech.com

Mechanical asymmetry during articulation of tibial and femoral cartilages: Local and overall compressive and shear deformation and properties

Benjamin L. Wong, Robert L. Sah *

Department of Bioengineering, Mail Code 0412, University of California—San Diego, 9500 Gilman Drive, La Jolla, CA 92093-0412, USA

ARTICLE INFO

Article history:
Accepted 26 February 2010

Keywords:
Cartilage
Biomechanics
Compression
Shear
Tibial–femoral articulation

ABSTRACT

During knee movement, femoral cartilage articulates against cartilage from the tibial plateau, and the resulting mechanical behavior is yet to be fully characterized. The objectives of this study were to determine (1) the overall and depth-varying axial and shear strains and (2) the associated moduli, of femoral and tibial cartilages during the compression and shearing of apposing tibial and femoral samples. Osteochondral blocks from human femoral condyles (FCs) characterized as normal and donor-matched lateral tibial plateau (TP) were apposed, compressed 13%, and subjected to relative lateral motion. When surfaces began to slide, axial ($-E_{zz}$) and shear (E_{xz}) strains and compressive (E) and shear (G) moduli, overall and as a function of depth, were determined for femoral and tibial cartilages. Tibial $-E_{zz}$ was ~2-fold greater than FC $-E_{zz}$ near the surface (0.38 versus 0.22) and overall (0.16 versus 0.07). Near the surface, E_{xz} of TP was 8-fold higher than that of FC (0.41 versus 0.05), while overall E_{xz} was 4-fold higher (0.09 versus 0.02). For TP and FC, $-E_{zz}$ and E_{xz} were greatest near the surface and decreased monotonically with depth. E for FC was 1.7-fold greater than TP, both near the surface (0.40 versus 0.24 MPa) and overall (0.76 versus 0.47 MPa). Similarly, G was 7-fold greater for FC (0.22 MPa) than TP near the surface (0.03 MPa) and 3-fold higher for FC (0.38 MPa) than TP (0.13 MPa) overall. These results indicate that tibial cartilage deforms and strains more axially and in shear than the apposing femoral cartilage during tibial–femoral articulation, reflecting their respective moduli.

1. Introduction

Femoral and tibial cartilages articulate against one other in the knee to biomechanically facilitate joint movement (Mow et al., 2005). During knee movement, cartilage lining the femoral condyle contacts, compresses, and slides against tibial cartilage (Fig. 1A). To reveal cartilage mechanical properties and deformation in response to loading, cartilage samples are typically tested *in vitro* and against non-biologic counter-platens in confined (Neu et al., 2005; Schinagl et al., 1997) and unconfined compression (Chahine et al., 2004; Jurvelin et al., 2003), torsion (Zhu et al., 1993), and shear (Buckley et al., 2008). Physiologically, a cartilage surface articulates against another cartilage surface, and the resulting deformation may depend on the mechanical behavior of the counter-articulating surface during mechanical tests. Therefore, mechanical tests that load physiologically apposing cartilage surfaces (i.e. femoral against tibial cartilage) would be useful to elucidate cartilage deformation, and its associated mechanical properties that occur during joint loading.

In response to physiologic loading, knee cartilage deforms, and the resulting strain magnitudes vary with joint location and tissue depth. Following various physical activities such as knee bending, impact loading, and running, cartilage compresses ~3–20% of the overall thickness (Eckstein et al., 2006; Kersting et al., 2005; Van de Velde et al., 2009), compression typically being higher in tibial than femoral cartilage (Eckstein et al., 2006; Kersting et al., 2005). Such differences in deformation between cartilage regions reflect differences in stiffness, with femoral cartilage being stiffer than tibial cartilage (Lyyra et al., 1999). Moreover, cartilage stiffness varies across the femoral (Athanasiou et al., 1991; Setton et al., 1994) and tibial (Mow et al., 2005) joint surfaces. During cartilage-on-cartilage articulation, axial and shear deformation of femoral cartilage varies with depth, being highest near the surface and becoming minimal near the tidemark (Wong et al., 2008a, 2008b). Collectively, these results suggest deformation of femoral and tibial cartilage is markedly different, overall and locally, during tibial–femoral articulation. While previous studies have elucidated local and overall femoral mechanical properties as well as overall tibial cartilage properties, local tibial compressive and shear mechanics remain to be investigated. Theoretical models of anatomic joint articulation can be used to predict local cartilage deformation (Ateshian et al., 1994; Swanson, 1979), but depend considerably on depth-varying

* Corresponding author. Tel: +1 858 534 0821; fax: +1 858 822 1614.
E-mail address: rsah@ucsd.edu (R.L. Sah).

0021-9290/$ - see front matter © 2010 Elsevier Ltd. All rights reserved.
doi:10.1016/j.jbiomech.2010.02.035

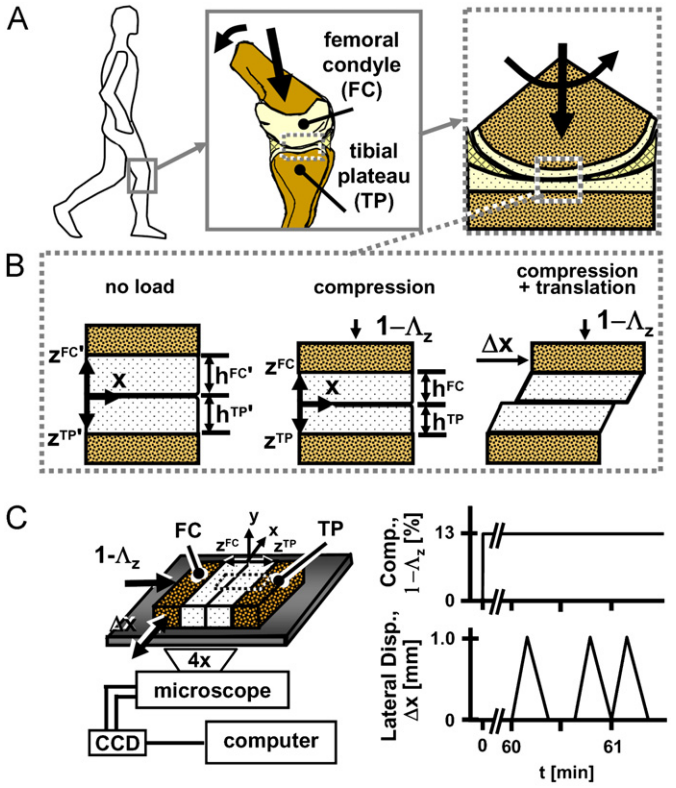

Fig. 1. Schematic of (A) knee joint movements at multiple scales and (B) deformation of cartilage under (from left to right) no load, compression, and compression+shear loading. Schematic of (C) experimental setup and loading protocol for micro-scale testing.

mechanical properties of the anatomical surfaces (Ateshian et al., 1994). Thus, a comprehensive characterization of femoral and tibial cartilage mechanical properties during tibial–femoral articulation, locally and overall, would further the understanding of cartilage mechanics.

Recently, cartilage deformation during cartilage-on-cartilage articulation was elucidated (Wong et al., 2008a, 2008b) using video microscopy (Schinagl et al., 1996) and image correlation to track the displacement of fiducial markers (Gratz and Sah, 2008; Wang et al., 2002). With this experimental approach, a pair of osteochondral blocks was compressed in apposition and subjected to lateral shearing motion to mimic the biomechanical environment during joint movement. The resulting compressive and shear strains of cartilage were determined locally and overall with a resolution sufficient to resolve small magnitudes ($\sim$1%) of strain. In addition, measurements of strain and stress were combined to determine local and overall shear moduli. However, such studies examined articulation mechanics in a simplified geometry, with the apposing cartilage samples being from the femoral condyle. Using this configuration, osteochondral samples from the tibial and femoral condyles can be apposed (Fig. 1B) and tested to examine the mechanics of tibial–femoral articulation (Fig. 1C) to extend previous findings and further the understanding of cartilage mechanics during joint movement.

Thus, the hypothesis of this study was that during tibial–femoral articulation, the deformation and associated properties of tibial cartilage are markedly different from those of the femoral cartilage. To test this hypothesis, the objectives of this study were to determine the overall and depth-varying axial and shear strains, as well as the associated overall and depth-varying moduli, of tibial and femoral cartilages during compression and shear.

2. Materials and methods

2.1. Sample preparation

Six osteochondral cores (each with a 10 mm diameter) were isolated, one each, from the anterior lateral femoral condyle (FC) of six fresh cadaveric human donors (mean $\pm$ SEM: 46 $\pm$ 1.5 yr). Additionally, six osteochondral blocks (each with a chondral area of $\sim$1 cm^2) were harvested from the region of the donor-matched lateral tibial plateau (TP) not covered by the meniscus. Femoral cores with grossly normal surfaces (modified Outerbridge of grade 1; Yamada et al., 2002) were selected, while all donor-matched tibial blocks displayed mild surface fibrillation and were of grades 2–3. The specimens were immersed in phosphate buffered saline (PBS) containing proteinase inhibitors (PIs; Frank et al., 1987) and stored at -70 °C until use.

2.2. Experimental design

On the day of testing, the osteochondral specimens were thawed and further processed. The femoral core and tibial block were each trimmed as previously (Wong et al., 2008a) using a low-speed saw (Isomet^{TM}, Buehler, Lake Bluff, IL) to yield an osteochondral fragment for histopathologic analysis (see Appendix A for description) and one $\sim$rectangular block for biomechanical testing. Each rectangular block had a cartilage surface area of $\sim 3 \times 8$ mm^2 and a total thickness of $\sim$1 cm. Paired femoral and donor-matched tibial blocks were created with the 8 mm lengths being parallel to the direction of joint articulation.

2.3. Biomechanical testing

Samples were first tested by micro-scale testing with PBS+PI as lubricant in a custom bi-axial loading chamber mounted onto an epi-fluorescence microscope for digital video (Fig. 1C) as previously described (Wong et al., 2008a) (See Appendix A for description). Following re-swelling at 4 °C for $\sim$16 h, femoral and tibial samples were then separately tested in a macro-scale system to assess overall cartilage mechanical properties as previously described (Wong et al., 2008a; see Appendix A for description).

2.4. Data analysis and statistics

To assess depth variation and compare strains computed from the digital micrographs (see Appendix A for description), local strains were averaged depthwise and plotted as a function of tissue depth. Sample thickness was normalized and divided into 8 intervals, with 4 intervals being 0.083 times the normalized thickness near the articular surface (i.e. 0–0.333) and 0.167 times for the remaining tissue depth (i.e. 0.333–1). To reduce noise and consolidate data, strains were averaged at the same normalized depth interval to yield a depth profile.

Overall axial and shear strains as well as the overall compressive (E) and shear moduli were determined as previously described (Wong et al., 2008a). For this study, shear moduli were determined relative to the compressed (G_1) and uncompressed (G_0) cartilage thickness. In addition, the depth-varying compressive and shear moduli were also estimated from the overall respective moduli and local strain for each sample (Wong et al., 2008a).

Data are reported as mean $\pm$ standard error of the mean (SEM). Repeated measures ANOVA was used to determine the effects of normalized tissue depth (0–1, surface bone) and location (FC, TP) on tissue strain and modulus. Planned pairwise comparisons were used to assess differences between FC and TP groups for strains and moduli near the surface and overall. Modulus data were log transformed before analysis to adjust for sample variances that were proportional to amplitude.

3. Results

3.1. Sample thickness and histopathology

Cartilage in TP samples was generally thicker than FCs, and the overall histopathology scores were consistent with their gross and histological appearances (Fig. 2). Tibial cartilage had an average thickness of 2.88 $\pm$ 0.53 mm, while femoral cartilage was 2.20 $\pm$ 0.15 mm in thickness. The histopathology score of 6.44 $\pm$ 0.72 for tibial samples was significantly higher ($p < 0.01$) than the femoral score of 1.83 $\pm$ 0.39. For tibial samples, structural features (surface irregularity and transverse clefts) exhibited mild degeneration and GAG loss was apparent, which

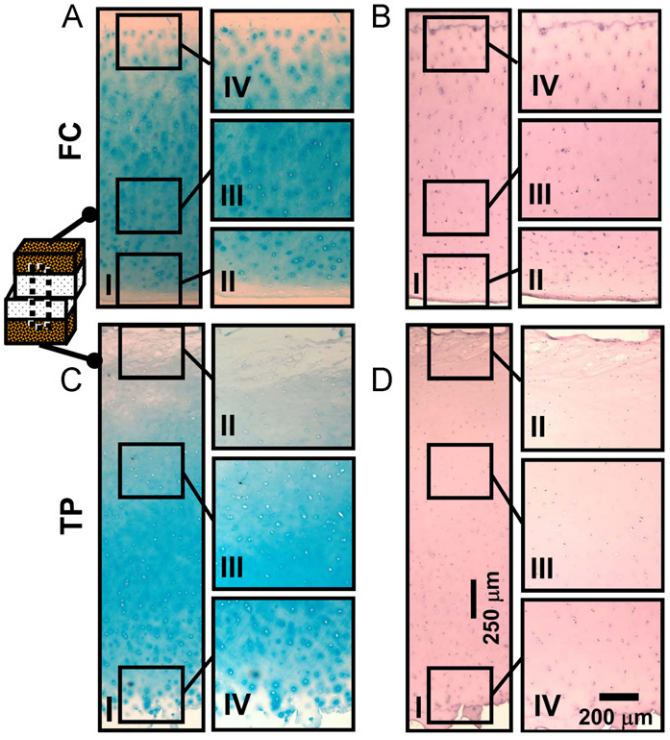

Fig. 2. Representative micrographs of femoral (FC, A, B) and tibial (TP, C, D) cartilages in apposition and stained with Alcian blue (A, C) and H&E (B, D) showing structural and cellular detail of the full thickness (I), superficial (II), middle (III), and deep (IV) regions. (For interpretation of the references to color in this figure legend, the reader is referred to the web version of this article.)

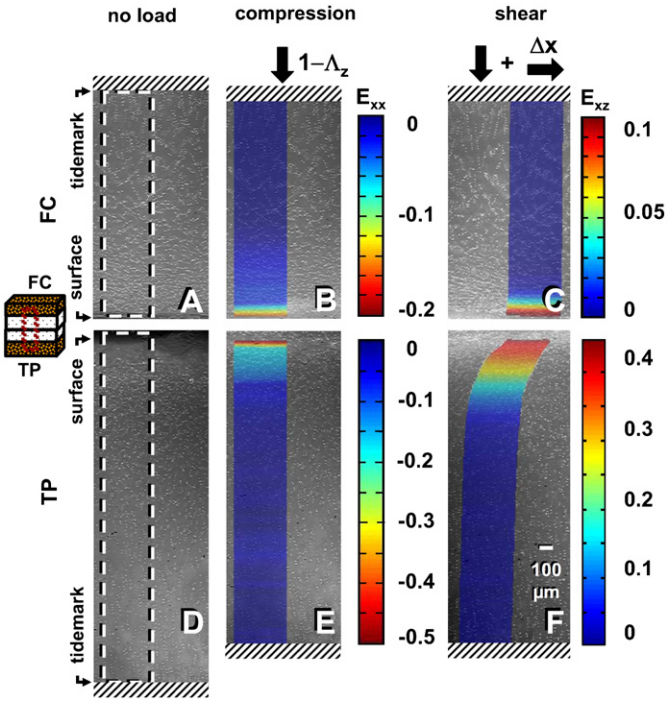

Fig. 3. Micrographs with superimposed strain color maps taken of apposing femoral (FC, A–C) to tibial (TP, D–F) samples when unloaded (A, D), after axial compression (B, E), and during lateral shear (C, F). Maps of compressive strain relative to the unloaded thickness (color maps: B, E) and shear strain relative to the compressed thickness (color maps, C, F) after achieving surface sliding were determined. Dashed lines (– –) encompass the analyzed regions on the undeformed images, while strain map boundaries encompass the corresponding deformed states. (For interpretation of the references to color in this figure legend, the reader is referred to the web version of this article.)

resulted in scores being ~1 point higher than those for femoral samples. In contrast, cellularity and cloning scores were similarly low (i.e. normal) between femoral and tibial samples.

3.1.1. Deformation: axial strains

At compressive equilibrium, $-E_{zz}$ decreased significantly with depth from the articular surface ($p<0.001$) for both locations (Fig. 3A, B, D, E) and was lower in magnitude in the FC (Fig. 3A, B) than TP cartilage (Fig. 3D, E). The axial displacements of the articular surface relative to the tidemark were on average 507 ± 92 and 169 ± 17 μm for TP and FC samples, respectively. This translated to $-E_{zz}$ near the articular surface being relatively high and decreasing markedly from 0.38 to 0.02 in the deepest regions for TP cartilage, and from 0.22 to 0.01 for FC samples (Fig. 4A). Near the articular surface, $-E_{zz}$ was ~2× higher ($p<0.01$) in TP (0.38) than FC (0.22) cartilage (Fig. 5A). Similarly, overall $-E_{zz}$ (nominal strain) of TP (0.16 ± 0.02) was twice that of

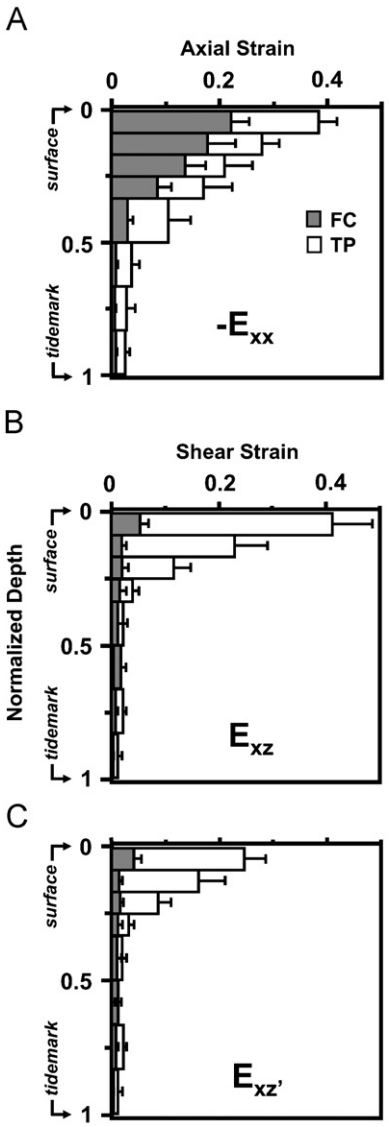

Fig. 4. Local compressive strain ($-E_{zz}$) relative to the unloaded cartilage thickness versus normalized tissue depth under applied compression alone (A) for both femoral (FC) and tibial (TP) cartilages. Local shear strain relative to the compressed cartilage thickness (E_{xz} in B) and to the unloaded cartilage thickness ($E_{xz'}$ in C) under compression and during shear. Values are mean ± SEM.

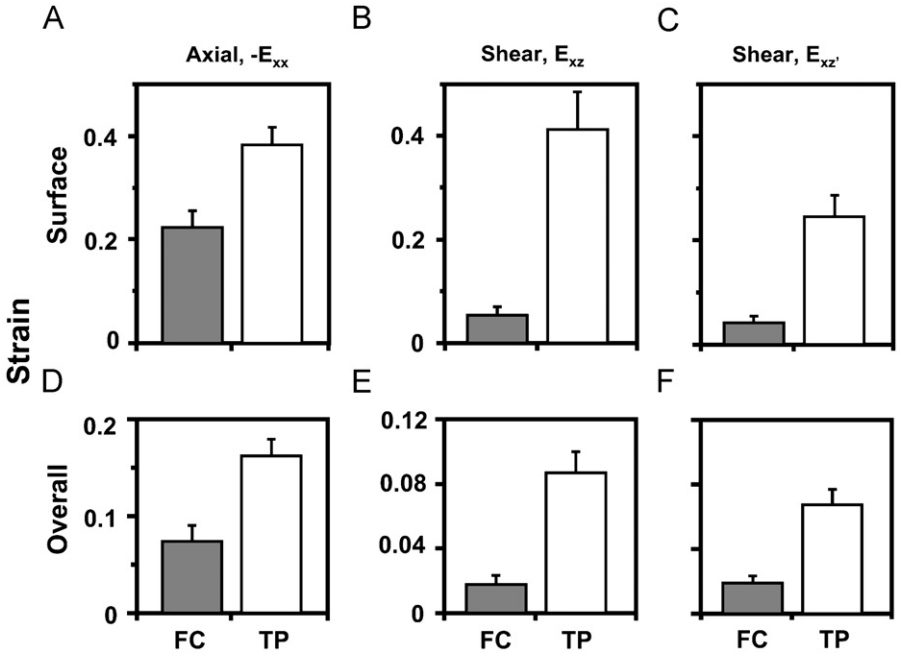

Fig. 5. Comparison of peak compressive ($-E_{zz}$) surface (A) and overall strains (D) relative to the unloaded cartilage thicknesses between femoral (FC) and tibial (TP) sample groups. Peak surface (B, C) and overall (E, F) shear strains relative to either the compressed cartilage thickness (*Exz* in B, E) or the unloaded cartilage thickness ($E_{xz'}$ in C, F).

FC (0.07 ± 0.02) cartilage (Fig. 5D). Lateral (E_{xx}) and shear (E_{xz}) strains resulting from the applied compression were low, averaging < 0.03 for all samples, while E_{xx} and $-E_{zz}$ did not apparently change following lateral motion ($< 1\%$; data not shown).

3.1.2. Deformation: shear strains

As described previously (Wong et al., 2008b), shear loading of apposing cartilage surfaces results in surface sliding with maintenance of peak shear deformation (Fig. 3C, F), and at this time, E_{xz} varied markedly with depth from the articular surface for both locations ($p < 0.01$) and between FC (Fig. 3C) and TP (Fig. 3F) cartilage ($p < 0.01$). On average, the resulting lateral displacements at the surface of TP and FC cartilage were 398 ± 38 and $81 \pm 9\,\mu m$, respectively. As a result, E_{xz} decreased significantly ($p < 0.001$) and monotonically from 0.41 and 0.05 near the articular surface, to very low magnitudes (≤ 0.01) near the tidemark for TP and FC cartilages, respectively (Fig. 4B). Near the articular surface, E_{xz} was $\sim 8\times$ higher ($p < 0.01$) in TP than FC cartilage (Fig. 5B), while overall E_{xz} (nominal strain) was $\sim 4\times$ higher ($p < 0.01$) for TP (0.09 ± 0.01) than FC (0.02 ± 0.01) samples (Fig. 5E). The effects of depth ($p < 0.01$) and tissue location ($p < 0.01$) on local (Figs. 4C, 5C) and overall (Fig. 5F) $E_{xz'}$ were similar to those found for E_{xz}; however, values were lower in magnitude.

3.1.3. Tissue properties: compressive

To estimate compressive loads during micro-scale tests, axial compression for each cartilage layer (FC, TP) in micro-scale shear tests was replicated by applying axial displacements measured in micro-scale tests (reported above) to FC and TP cartilages in macro-scale tests. As a function of normalized tissue depth, compressive modulus (E) was not apparently different between locations at all depths ($p = 0.11$) and near the articular surface ($p = 0.17$; Fig. 6A). Since cartilage thickness was generally greater in TP samples, each normalized depth interval was thicker for TP

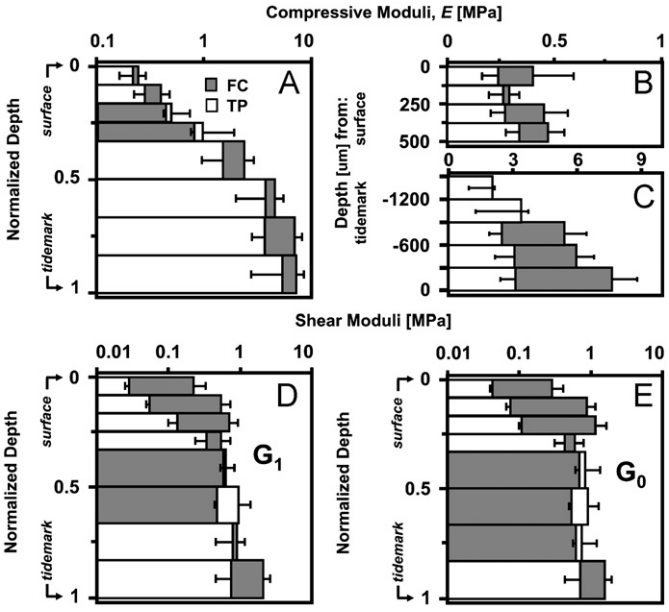

Fig. 6. Local compressive modulus (E) relative to the unloaded cartilage thickness versus normalized tissue depth (A), absolute depth from the articular surface (B), and tidemark (C) under applied compression alone for both femoral (FC) and tibial (TP) cartilages. Local shear modulus versus normalized tissue depth relative to the compressed cartilage thickness (G_1 in D) and to the unloaded cartilage thickness (G_0 in E) under compression and during shear. Values are mean $\pm$ SEM.

cartilage, and comparisons of E may be more appropriate between similar thickness depth regions. Within the top $125\,\mu m$ of the articular surface (Figs. 6B, 7A), E was 0.40 ± 0.19 MPa for FC cartilage, being markedly higher ($p < 0.05$) than that of TP samples (0.24 ± 0.08 MPa). Similarly, overall E was markedly higher ($p < 0.01$) for FC (0.76 ± 0.13 MPa) than TP cartilage (0.47 ± 0.08 MPa; Fig. 7D).

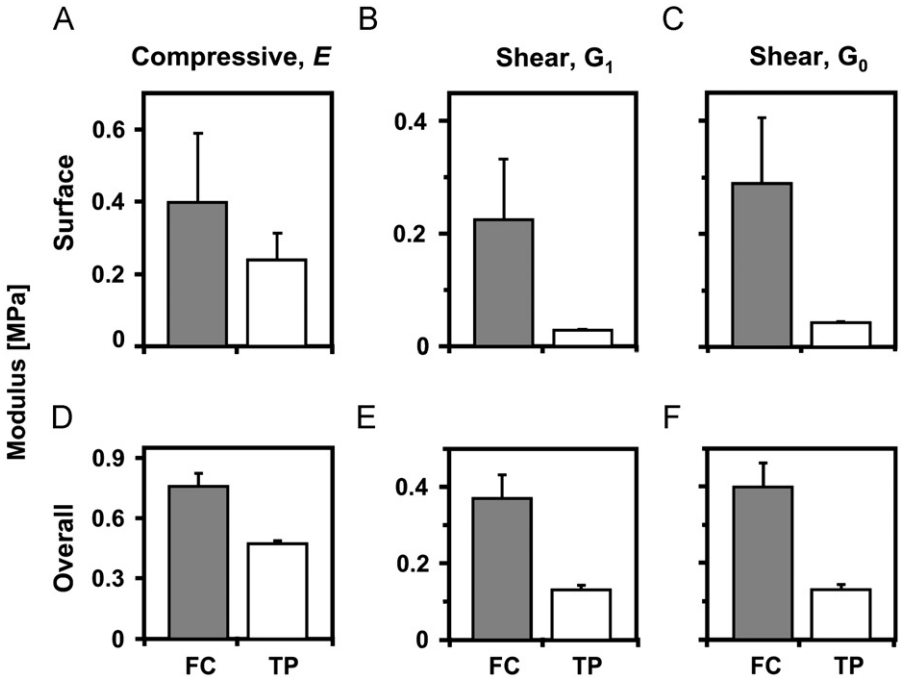

Fig. 7. Comparison of peak compressive (E) surface (A) and overall moduli (D) relative to the unloaded cartilage thicknesses between femoral (FC) and tibial (TP) sample groups. Peak surface (B, C) and overall (E, F) shear moduli relative to either the compressed cartilage thickness (G_1 in B, E) or the unloaded cartilage thickness (G_0 in C, F).

3.1.4. Tissue properties: shear

For measurements of shear loads, the resulting shear deformation of each cartilage layer (FC, TP) in micro-scale tests was replicated in macro-scale tests by applying resulting lateral surface displacement measured from micro-scale tests (reported above) to FC and TP cartilages. For FC cartilage, shear modulus relative to the compressed cartilage thickness (G_1) near the surface was 0.22 ± 0.11 MPa, which was 7-fold higher ($p < 0.05$) than the surface G_1 of TP cartilage (0.03 ± 0.003 MPa; Figs. 6D, 7B). Overall G_1 was markedly higher ($p < 0.001$) in FC (0.38 ± 0.06 MPa) than TP cartilage (0.13 ± 0.01 MPa; Fig. 7E). The effect of location on local (Figs. 6D, 7C) and overall (Fig. 7G) shear moduli relative to the uncompressed thickness (G_0) was found to be similar to that of G_1, G_0 being markedly higher in FC cartilage near the surface ($p < 0.01$) and overall ($p < 0.001$). In all cases, values of G_0 were slightly higher in magnitude than G_1.

4. Discussion

This study utilized a micro-scale cartilage-on-cartilage testing system to elucidate cartilage strain during tibial–femoral articulation as well as the mechanical properties of femoral and tibial cartilages. The present results indicate that during axial and lateral loading of tibial against femoral cartilage (Fig. 8A), tibial cartilage deforms and strains markedly more in both compression and shear than femoral cartilage (Fig. 8B), and such trends are a result of femoral cartilage being stiffer in compression and shear. Under axial displacement, tibial $-E_{zz}$ was 0.38 near the articular surface and 0.16 overall, being 50% higher than femoral $-E_{zz}$ (surface -0.22; overall -0.07). During lateral motion, tibial E_{xz} was 0.41 near the surface and 0.09 overall, being ~80% higher than that of FC (surface -0.05; overall -0.02). In addition, E near the surface and overall for FC were both ~40% higher than that of TP. Analogously, G_1 and G_0 were greater in magnitude for FC than TP, being 80% higher near the surface and 65% overall.

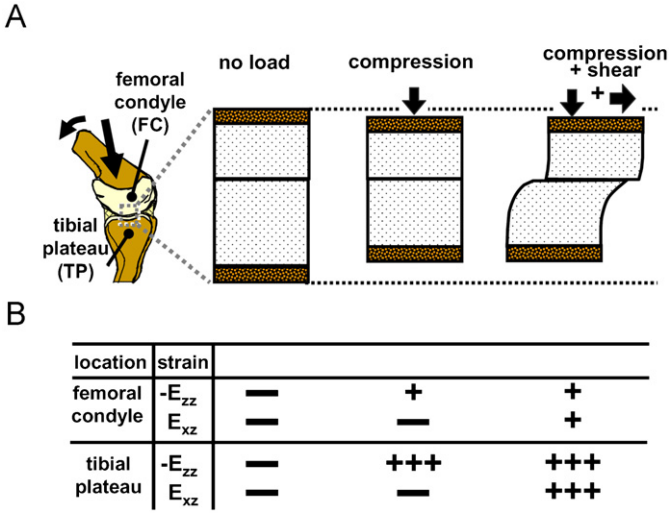

Fig. 8. (A) Schematic of cartilage compressive and shear deformations of femoral cartilage apposing tibial cartilage when unloaded, compressed, and compressed and sheared. (B) Table of relative magnitudes for compressive ($-E_{zz}$) and shear strain (Exz) for both femoral and tibial cartilages when they are unloaded, compressed, and compressed and sheared in apposition.

The experimental approach utilized in the present study mimics the compression and sliding between femoral and tibial cartilage that occurs during physiologic tibial–femoral joint articulation. Samples were taken from the load bearing regions of the lateral femoral condyle and donor-matched tibial plateau, where such surfaces appose and articulate against each other anatomically (Mow et al., 2005). Such regions experience a wide range of compression (3–20%; Eckstein et al., 2006; Kersting et al., 2005; Van de Velde et al., 2009) and sliding (up to ~50 mm) during normal activities (estimated from Whittle, 2002;

Shelburne et al., 2005). The present study addresses certain physiologic loading parameters (i.e. high compressive loading and low sliding velocity during contralateral toe-off and heel rise; Whittle, 2002) as well as the relative loading and sliding of physiologically articulating cartilage surfaces. Furthermore, shear moduli and strain were determined for a part of the gait cycle, with high compression and low sliding rate, that likely initiated a relatively large interaction between two opposing tissue surfaces. Since samples were stress relaxed for 1 h, the resulting deformation and strains are likely representative of those occurring following prolonged cyclic loading of the femoral and tibial surfaces (i.e. prolonged running, walking, etc.). With prolonged cyclic compression, cartilage gradually depressurizes and eventually reaches a steady-state compression. Furthermore, certain regions of the femoral joint are in constant contact with an apposing articular surface during cyclic loading, and the present results for femoral cartilage would likely be representative for such regions.

Boundary conditions of the present study provide insight on the effect of pathophysiologic lubrication on cartilage deformation. While conditions [1 h stress relaxation and relatively high overall compressive strain ($\sim$13%)] that result in cartilage boundary lubrication (Schmidt and Sah, 2007) were utilized, overall compressive strain was much greater in tibial than femoral cartilage, and thus, the resulting lubrication mode between the two surfaces, which may be mixed mode and/or boundary, would be difficult to discern due to this asymmetry. Furthermore, synovial fluid (SF) normally lubricates surfaces physiologically and reduces absolute magnitudes of E_{xz} during articulation in the boundary mode (Wong et al., 2008a, 2008b); the present study used PBS as a lubricant to allow sufficient lateral displacements in femoral samples so that G_1 could be appropriately estimated. In addition, such a condition mimics impaired SF function and gives insight on the effect of pathophysiologic lubrication on cartilage deformation. However, relative differences in strain and modulus between regions should be consistent, although measured E_{xz} would likely be reduced if SF had been used (Wong et al., 2008a). Future studies could be conducted to assess the effects of normal and abnormal lubricants on cartilage deformation during tibial–femoral articulation.

Depth variations in $-E_{zz}$, E_{xz}, E, and G_1 for the cartilage used in this study are consistent with those previously reported. In both compressed tibial (Neu et al., 2005) and patella–femoral cartilage (Schinagl et al., 1997), $-E_{zz}$ was depth-varying, decreasing monotocially with increasing depth from the articular surface. During lateral articulation, E_{xz} was also the highest at articular surface and the lowest near the tidemark (Wong et al., 2008a, 2008b) in femoral cartilage. For the present study, both $-E_{zz}$ and E_{xz} of femoral and tibial cartilages exhibited similar depth-varying trends (Fig. 4), decreasing markedly with increasing depth. Reflective of the depth variation in strain, cartilage stiffness in compression (Schinagl et al., 1997) and shear (Wong et al., 2008a) for patella–femoral and femoral cartilage, respectively, increased with increasing depth. Similarly, E and G_1 for femoral and tibial cartilages both increased with increasing depth, being $\sim$1.5–2 $\times$ lower near the surface and 5–10 $\times$ higher near the tidemark than the overall values (Fig. 5). Since shear loads were measured at a lateral strain after 10 s, G_1 determined in the present study indicates the cartilage shear stiffness after $\sim$0.8 mm of relative surface motion, being $\sim$10–50% higher than that at equilibrium (Spirt et al., 1989).

In contrast with the present results, G_1 was found to be the lowest just beneath the superficial zone in cartilage in a recent study (Buckley et al., 2008). This may stem from differences in the methodologies employed, which include the method to induce shear and the resolution of presented data. In the previous study, sliding did not occur between cartilage and platen surfaces since a platen was gripped to the articular surface and displaced laterally to induce shear. In the present study, shear behavior was determined when unbound cartilage surfaces were sliding relative to one another. The presence of sliding may further drag the superficial tissue and induce shear strains to be the greatest at the surface and result in the depth variation in shear modulus observed in the present study. In addition, the resolution of the present data ($\sim$100–150 μm near the surface) is lower than that of the previous study ($\sim$40 μm), which could possibly mask peaks just beneath the surface (0–100 μm). Future investigations may clarify the reasons for these differences.

The magnitudes of E and G_1 reported in this study for cartilage from human femoral condyles and tibial plateau are consistent with those previously reported. From indentation tests, overall E was estimated to be 0.47 and 0.68 MPa for cartilage from the lateral aspects of the tibial plateau and femoral condyle, respectively (Lyyra et al., 1999), being similar to those found in the current study (TP: 0.47 MPa, FC: 0.76 MPa). Analogous to E, overall G_1 for femoral cartilage reported for this study (0.38 MPa) is also consistent with those previously reported (0.32 MPa; Wong et al., 2008a). Thus, for human tibial–femoral cartilage, mechanical properties in compression and shear are similar to those previously described.

The tissue deformation being greater in cartilage from the tibia than the femoral condyle is consistent with *in vivo* tibial–femoral deformation and predictions accounting for past studies on tibial and femoral tissue stiffness. Following impact loading, tibial cartilage deformation was observed with MRI to be significantly higher than that of femoral cartilage (Eckstein et al., 2006). In addition, indentation stiffness for femoral cartilage was $\sim$1.2–1.5 times greater than for tibial cartilage in human joints (Lyyra et al., 1999), being consistent with trends (1.5–2 times) found in this study. As a result, femoral cartilage would be predicted to deform less than tibial cartilage during articulation because it is relatively stiffer. In addition to the intrinsic structural differences between regions (Arokoski et al., 1999), differences in deformation, and associated stiffness, may be partly attributed to the mild degeneration observed in tibial cartilage (Fig. 2). Since the region of tibial cartilage that is uncovered by the meniscus typically shows signs of early degeneration (Bennett et al., 1942) and femoral cartilage typically displays signs of degeneration in elder individuals ($>$60 yrs old), the present results would be representative for that of a normal mature adult.

This study further elucidates cartilage mechanics by providing insight on the cartilage deformation of articulating surfaces during tibial–femoral joint articulation. Collectively, the present results suggest cartilage deformations in compression and shear are asymmetric between cartilage surfaces, locally and overall, during tibial–femoral articulation, being markedly higher in tibial cartilage than in femoral cartilage, and are reflected by differences in mechanical stiffness. Cell metabolism and matrix synthesis, and as a result tissue structure, are markedly regulated by mechanical deformation (Jin et al., 2001; Nugent et al., 2006; Sah et al., 1989). Thus, relative differences in deformation between articulating surfaces may be a biomechanical stimulus that regulates regional variations in cartilage stiffness, as well as the metabolic and cellular responses to maintain homeostasis normally and in injury, within the physiologic knee joint.

Conflict of interest

The authors have no conflicts of interest to report.

Acknowledgements

This work was supported by NIH and Howard Hughes Medical Institute through the Professors Program Grant to UCSD for Dr. Robert L. Sah. We thank the many residents and staff at Dr. Lotz's Laboratory at the Scripps Research Institute for harvesting and providing the human tissue used in this study, and Chris Kim and Dr. Won Bae for their help in the histopathology assessments.

Appendix A. Supplementary material

Supplementary data associated with this article can be found in the online version at doi:10.1016/j.biomech.2010.02.035.

References

Arokoski, J.P., Hyttinen, M.M., Helminen, H.J., Jurvelin, J.S., 1999. Biomechanical and structural characteristics of canine femoral and tibial cartilage. J Biomed Mater Res 48, 99–107.

Ateshian, G.A., Lai, W.M., Zhu, W.B., Mow, V.C., 1994. An asymptotic solution for the contact of two biphasic cartilage layers. J. Biomech. 27, 1347–1360.

Athanasiou, K.A., Rosenwasser, M.P., Buckwlter, J.A., Malinin, T.I., Mow, V.C., 1991. Interspecies comparisons of in situ intrinsic mechanical properties of distal femoral cartilage. J. Orthop. Res. 9, 330–340.

Bennett, G.A., Waine, H., Bauer, W., 1942. Changes in the knee joint at various ages with particular reference to the nature and development of degenerative joint disease. The Commonwealth Fund, New York.

Buckley, M.R., Gleghorn, J.P., Bonassar, L.J., Cohen, I., 2008. Mapping the depth dependence of shear properties in articular cartilage. J. Biomech. 41, 2430–2437.

Chahine, N.O., Wang, C.C., Hung, C.T., Ateshian, G.A., 2004. Anisotropic strain-dependent material properties of bovine articular cartilage in the transitional range from tension to compression. J. Biomech. 37, 1251–1261.

Eckstein, F., Hudelmaier, M., Putz, R., 2006. The effects of exercise on human articular cartilage. J. Anat. 208, 491–512.

Frank, E.H., Grodzinsky, A.J., Koob, T.J., Eyre, D.R., 1987. Streaming potentials: a sensitive index of enzymatic degradation in articular cartilage. J. Orthop. Res. 5, 497–508.

Gratz, K.R., Sah, R.L., 2008. Experimental measurement and quantification of frictional contact between biological surfaces experiencing large deformation and slip. J. Biomech. 41, 1333–1340.

Jin, M., Frank, E.H., Quinn, T.M., Hunziker, E.B., Grodzinsky, A.J., 2001. Tissue shear deformation stimulates proteoglycan and protein biosynthesis in bovine cartilage explants. Arch. Biochem. Biophys. 395, 41–48.

Jurvelin, J.S., Buschmann, M.D., Hunziker, E.B., 2003. Mechanical anisotropy of the human knee articular cartilage in compression. Proc. Inst. Mech. Eng. H 217, 215–219.

Kersting, U.G., Stubendorff, J.J., Schmidt, M.C., Bruggemann, G.P., 2005. Changes in knee cartilage volume and serum comp concentration after running exercise. Osteoarthritis Cartilage 13, 925–934.

Lyyra, T., Kiviranta, I., Vaatainen, U., Helminen, H.J., Jurvelin, J.S., 1999. In vivo characterization of indentation stiffness of articular cartilage in the normal human knee. J. Biomed. Mater. Res. 48, 482–487.

Mow, V.C., Gu, W.Y., Chen, F.H., 2005. Structure and function of articular cartilage and meniscus. In: Mow, V.C., Huiskes, R. (Eds.), Basic Orthopaedic Biomechanics and Mechano-biology.. Lippincott Williams & Wilkins, Philadelphia, pp. 720.

Neu, C.P., Hull, M.L., Walton, J.H., 2005. Heterogeneous three-dimensional strain fields during unconfined cyclic compression in bovine articular cartilage explants. J. Orthop. Res. 23, 1390–1398.

Nugent, G.E., Aneloski, N.M., Schmidt, T.A., Schumacher, B.L., Voegtline, M.S., Sah, R.L., 2006. Dynamic shear stimulation of bovine cartilage biosynthesis of proteoglycan 4 (prg4). Arthritis Rheum. 54, 1888–1896.

Sah, R.L., Kim, Y.J., Doong, J.H., Grodzinsky, A.J., Plaas, A.H.K., Sandy, J.D., 1989. Biosynthetic response of cartilage explants to dynamic compression. J. Orthop. Res. 7, 619–636.

Schinagl, R.M., Gurskis, D., Chen, A.C., Sah, R.L., 1997. Depth-dependent confined compression modulus of full-thickness bovine articular cartilage. J. Orthop. Res. 15, 499–506.

Schinagl, R.M., Ting, M.K., Price, J.H., Sah, R.L., 1996. Video microscopy to quantitate the inhomogeneous equilibrium strain within articular cartilage during confined compression. Ann. Biomed. Eng. 24, 500–512.

Schmidt, T.A., Sah, R.L., 2007. Effect of synovial fluid on boundary lubrication of articular cartilage. Osteoarthritis Cartilage 15, 35–47.

Setton, L.A., Mow, V.C., Muller, F.J., Pita, J.C., Howell, D.S., 1994. Mechanical properties of canine articular cartilage are significantly altered following transection of the anterior cruciate ligament. J. Orthop. Res. 12, 451–463.

Shelburne, K.B., Torry, M.R., Pandy, M.G., 2005. Muscle, ligament, and joint-contact forces at the knee during walking. Med. Sci. Sports Exerc. 37, 1948–1956.

Spirt, A.A., Mak, A.F., Wassell, R.P., 1989. Nonlinear viscoelastic properties of articular cartilage in shear. J. Orthop. Res. 7, 43–49.

Swanson, S.A.V., 1979. Friction, wear, and lubrication. In: Freeman, M.A.R. (Ed.), Adult Articular Cartilage. Pitman Medical, Tunbridge Wells, England, pp. 415–460.

Van de Velde, S.K., Bingham, J.T., Gill, T.J., Li, G., 2009. Analysis of tibiofemoral cartilage deformation in the posterior cruciate ligament-deficient knee. J. Bone Joint Surg. Am. 91, 167–175.

Wang, C.C., Deng, J.M., Ateshian, G.A., Hung, C.T., 2002. An automated approach for direct measurement of two-dimensional strain distributions within articular cartilage under unconfined compression. J. Biomech. Eng. 124, 557–567.

Whittle, M., 2002. Gait Analysis: An Introduction. Butterworth-Heinemann, Oxford; Boston.

Wong, B.L., Bae, W.C., Chun, J., Gratz, K.R., Lotz, M., Sah, R.L., 2008a. Biomechanics of cartilage articulation: effects of lubrication and degeneration on shear deformation. Arthritis Rheum. 58, 2065–2074.

Wong, B.L., Bae, W.C., Gratz, K.R., Sah, R.L., 2008b. Shear deformation kinematics during cartilage articulation: effect of lubrication, degeneration, and stress relaxation. Mol. Cell. Biomech. 5, 197–206.

Yamada, K., Healey, R., Amiel, D., Lotz, M., Coutts, R., 2002. Subchondral bone of the human knee joint in aging and osteoarthritis. Osteoarthritis Cartilage 10, 360–369.

Zhu, W., Mow, V.C., Koob, T.J., Eyre, D.R., 1993. Viscoelastic shear properties of articular cartilage and the effects of glycosidase treatment. J. Orthop. Res. 11, 771–781.